



Crystal Structure of the Phage T4 Recombinase UvsX and Its Functional Interaction with the T4 SF2 Helicase UvsW

Stefan Gajewski^{1,2}, Michael R. Webb³, Vitold Galkin⁴,
Edward H. Egelman⁴, Kenneth N. Kreuzer^{3*} and Stephen W. White^{1,5*}

¹Department of Structural Biology, St. Jude Children's Research Hospital, 262 Danny Thomas Place, Memphis, TN 38105, USA

²Institut für Molekulare Biowissenschaften, Karl Franzens Universität, Humboldtstrasse 50/3, A-8010 Graz, Austria

³Department of Biochemistry, Duke University Medical Center, Nanaline Duke, Durham, NC 27710, USA

⁴Department of Biochemistry and Molecular Genetics, University of Virginia, Charlottesville, VA 22908, USA

⁵Department of Molecular Sciences, University of Tennessee Health Science Center, Memphis, TN 38163, USA

Received 23 July 2010;
received in revised form
1 October 2010;
accepted 6 October 2010
Available online
28 October 2010

Edited by R. Huber

Keywords:

DNA repair;
recombination;
RecA;
electron microscopy;
X-ray crystallography

Bacteriophage T4 provides an important model system for studying the mechanism of homologous recombination. We have determined the crystal structure of the T4 UvsX recombinase, and the overall architecture and fold closely resemble those of RecA, including a highly conserved ATP binding site. Based on this new structure, we reanalyzed electron microscopy reconstructions of UvsX–DNA filaments and docked the UvsX crystal structure into two different filament forms: a compressed filament generated in the presence of ADP and an elongated filament generated in the presence of ATP and aluminum fluoride. In these reconstructions, the ATP binding site sits at the protomer interface, as in the RecA filament crystal structure. However, the environment of the ATP binding site is altered in the two filament reconstructions, suggesting that nucleotide cannot be as easily accommodated at the protomer interface of the compressed filament. Finally, we show that the phage helicase UvsW completes the UvsX-promoted strand-exchange reaction, allowing the generation of a simple nicked circular product rather than complex networks of partially exchanged substrates.

© 2010 Elsevier Ltd. All rights reserved.

*Corresponding authors. S. W. White, Department of Structural Biology, St. Jude Children's Research Hospital, 262 Danny Thomas Place, Mail Stop 311, Memphis, TN 38105-3678, USA; K. N. Kreuzer, Department of Biochemistry, Duke University Medical Center, Nanaline Duke, Room 157, Durham, NC 27710, USA. E-mail addresses: kenneth.kreuzer@duke.edu; stephen.white@stjude.org.

Abbreviations used: HJ, Holliday junction; ssDNA, single-stranded DNA; dsDNA, double-stranded DNA; EM, electron microscopy; RMP, recombination mediator protein; SAD, single-wavelength anomalous dispersion; SeMet, selenomethionine; IHRSR, Iterative Helical Real-Space Reconstruction; EDTA, ethylenediaminetetraacetic acid.

Introduction

Homologous recombination is a key process in DNA metabolism.^{1,2} Simple cut-and-paste mechanisms for recombination involve the alignment of the homologous regions of two DNA molecules, strand exchange, formation of a Holliday junction (HJ), HJ branch migration, and HJ resolution. In addition, homologous recombination pathways often involve DNA replication events (either localized or extensive) where DNA polymerase and associated proteins gain access to the invading 3' end within a recombination intermediate. Although homologous recombination is typically associated with the generation of genetic

diversity, it has critical roles in DNA repair³ and in the rescue of stalled and collapsed replication forks.⁴

The central protein in strand exchange is the recombinase (e.g., bacterial RecA) that cooperatively and nonspecifically polymerizes on single-stranded DNA (ssDNA) and forms helical filaments that bind double-stranded DNA (dsDNA). Subsequent events include homology search, alignment of homologous regions, and strand exchange using an ATP-dependent mechanism.^{1,5} The structural basis for homologous strand pairing and exchange, although relatively well understood biochemically, has yet to be fully elucidated. Electron microscopy (EM) and single-molecule studies have provided important insights,^{6–8} and crystallographic studies have now revealed how RecA molecules interact with individual and paired ssDNA molecules within the filament.⁹

Bacteriophage T4 is an attractive system for studying recombination and DNA metabolism in general. The majority of T4 DNA replication occurs by a recombination-dependent mechanism, allowing a detailed study of the coupling of replication and recombination.¹⁰ Invasive ssDNA ends are prepared for recombination by the exonuclease complex encoded by phage genes 46 and 47,¹¹ and the subsequent recombination process is apparently mediated by just four proteins: the recombinase UvsX, the recombination mediator protein (RMP) UvsY, the ssDNA-binding protein gp32,¹² and the branch-specific helicase UvsW.

UvsX is a 44-kDa RecA-like protein that forms similar helical assemblies on ssDNA^{13,14} and promotes joint molecule formation between homologous dsDNA molecules and homologous ssDNA molecules.^{15–18} UvsX utilizes an accessory protein, UvsY, to form stable filaments. UvsY is classified as an RMP,¹⁹ stimulates the ssDNA-dependent ATPase activity of UvsX, and lowers the critical concentration of UvsX required for activity.^{19–21} The interaction between UvsX and UvsY displaces the T4 ssDNA-binding protein gp32 from ssDNA prior to filament formation.^{22–24} UvsX and UvsY are functionally homologous to the eukaryotic Rad51 and Rad52 proteins, respectively.¹⁹

UvsW is a 58-kDa SF2 helicase that unwinds branched DNA molecules, including static X structures resembling HJs.^{25,26} The UvsW helicase has multiple roles in T4 DNA replication, recombination, and repair.^{25,27–29} The biochemical properties of UvsW have been extensively characterized,^{30,31} and we have determined its crystal structure.^{32,33}

Here we report the crystal structure of a large fragment of UvsX and demonstrate its close structural and functional similarities to RecA. We also demonstrate that the structure can be fitted into image reconstructions of the active UvsX filament obtained from EM in a manner consistent

with the published RecA active filament structure.⁹ Finally, we present direct evidence for a central role of UvsW helicase in promoting strand-exchange reaction.

Results

Fragment characterization and structure determination of UvsX

To initiate crystallization trials, we purified the full-length UvsX (UvsX_{1–391}) as a 6×His-tagged fusion protein, with four additional residues remaining at the N-terminus after cleavage with thrombin. It was necessary to add reducing agents to concentrate the protein to higher than 5 mg/ml. Two UvsX species of lower molecular mass were consistently present when the concentrated protein was analyzed using SDS-PAGE. Mass spectrometry revealed that one species was missing 15 residues at the N-terminus and that the other was lacking an additional 32 residues at the C terminus. Based on further fragment analysis using limited trypsin digestion and mass spectrometry, together with sequence comparison with RecA, three additional constructs were prepared for crystallization trials: residues 1–358 (UvsX_{1–358}), residues 30–391 (UvsX_{30–391}), and residues 30–358 (UvsX_{30–358}). Only UvsX_{30–358} yielded crystals, and many conditions were eventually identified between pH 7.0 and pH 9.5. However, all crystals were morphologically similar and belonged to space group $P6_1$ with cell dimensions $a=b=96.0$ Å, and $c=131.3$ Å.

The initial structure from selenomethionine (SeMet)-labeled crystals was determined using single-wavelength anomalous dispersion (SAD) techniques at 2.8 Å resolution, and the electron density map allowed a complete tracing of the molecule, which revealed two monomers in the asymmetric unit. The final structure was refined at 2.4 Å using native data, and the data collection and refinement statistics are shown in Table 1. In chain A, residues 152–165, 197–211, 228–237, and 341–358 were not visible in the electron density map and were omitted from the structure. In addition, the side chains of residues 35, 151, 226–227, 238, 261–263, 286, 297, 301, and 307 were not defined and built as alanines. In chain B, residues 152–166, 198–211, 228–238, and 343–358 were omitted, and residues 31, 35, 151, 226–227, 261–263, 286, and 307 were built as alanines.

Crystal structure of dimeric UvsX_{30–358}

The two molecules in the asymmetric unit are virtually identical apart from loop regions and superimpose with an RMSD on C $^{\alpha}$ atoms of

Table 1. Crystallographic data collection and refinement statistics of UvsX_{30–358}

	Native	SAD
<i>Data collection</i>		
Wavelength (Å)	1.0	0.97931
Space group	<i>P</i> 6 ₁	<i>P</i> 6 ₁
Unit cell parameters <i>a</i> , <i>b</i> , <i>c</i> (Å)	96.0, 96.0, 131.3	95.5, 95.5, 132.3
Resolution (Å)	83.04–2.35	50–2.8
Mosaicity (°)	0.549	1.157
Unique reflections	28,005	16,391
Redundancy	7.9	14.4
Completeness (%) ^a	99.3 (92.8)	97.2 (81.2)
<i>I</i> / σ ^{a,b}	29.5 (3.2)	27.4 (2.1)
<i>R</i> _{sym} (%) ^{a,c}	5.9 (34.5)	11.6 (44.9)
<i>Refinement</i>		
<i>R</i> _{crystal} / <i>R</i> _{free} (%) ^{a,d}	21.0/24.8 (31.1/36.3)	
Average <i>B</i> -factors (Å ²)		
Chain A (Protein)	23.08	
Chain B (Protein)	23.13	
Chain C (Water)	28.40	
Chain D (PO ₄)	42.43	
Ramachandran (%)		
Favored	92.2	
Allowed	7.8	
Outliers	0	
RMSD		
Bond length (Å)	0.018	
Bond angle (°)	1.759	
Chirality	0.127	

^a Values in parentheses are from the highest-resolution shell.

^b *I*/ σ is the mean reflection intensity divided by the estimated error.

^c $R_{\text{sym}} = (\sum |I_{hkl} - \langle I \rangle|) / (\sum I_{hkl})$, where the average intensity $\langle I \rangle$ is taken over all symmetry equivalent measurements, and I_{hkl} is the measured intensity for any given reflection.

^d $R_{\text{crystal}} = \frac{||F_o| - |F_c||}{|F_o|}$, where F_o and F_c are the observed and calculated structure factor amplitudes, respectively. R_{free} is equivalent to R_{crystal} but is calculated for 5% of the reflections chosen at random and omitted from the refinement process.

0.44 Å. The molecule contains a larger N-terminal ('core') $\alpha\beta$ domain and a smaller C-terminal domain with a mainly α -helical structure (Fig. 1a). The core domain contains a mixed eight-stranded β -sheet in which strands β 3 (residues 109–115), β 2 (83–91), β 4 (137–144), β 5 (189–195), β 1 (55–60), and β 6 (220–226) are parallel, and strands β 7 (239–246) and β 8 (253–261) form a β -hairpin that associates with strand β 6 and leads into the C-terminal domain. The β -sheet is flanked by two long α -helices on one side (α 4, 118–131; α 5, 168–186) and by two more α -helices on the opposite side (α 1, 37–44; α 2, 66–80), together with the C-terminal domain. In common with other RecA-like structures that do not contain DNA, residues within loops L1 (152–165) and L2 (198–211) are unstructured. The C-terminal domain contains a small three-stranded β -sheet (β 9, 281–285; β 10, 290–297; β 11, 300–306) in which strands β 10 and β 11 create an extended β -hairpin.

This β -sheet is exposed on the surface of UvsX, and three α -helices in the domain (α 8, 272–279; α 9, 317–325; α 10, 326–337) pack against the core domain. Residues 342–358 at the C-terminus of our construct are not visible in the electron density map. Despite the relatively poor sequence conservation,³⁵ the overall fold of UvsX_{30–358} closely resembles that of the equivalent fragment of RecA (residues 39–333) (Fig. 1b and c).

The two monomers in the asymmetric unit are related by a local 2-fold axis and interact via two surfaces, one on each domain (Fig. 2a). The larger surface on the core domain (1334 Å²) is centered on residues Phe65, Arg79, Tyr99, and Met103, and the smaller interaction surface on the C-terminal domain (357 Å²) is centered on Cys316 and Thr317. The electron density of the paired Cys316 side chains suggests that a fraction of the dimers in the crystal are connected by a disulfide bond. To test whether the disulfide bond can exist in solution, we analyzed the full-length UvsX and the three truncated versions by nonreducing SDS-PAGE (Fig. 3a). Samples were extensively dialyzed to remove all reducing agents and then fully oxidized using 1% H₂O₂. In all four constructs, a significant fraction of the protein appeared as a band of twice the molecular mass that was confirmed as UvsX by mass spectrometry, and this higher-molecular-mass band disappeared after the addition of 5 mM tris (2-carboxyethyl) phosphine as reducing agent. UvsX_{1–391}, UvsX_{30–391}, and UvsX_{1–358} all showed a similar ratio of dimers to monomers under oxidizing solution conditions (approximately one-half), whereas the dimeric species was less prominent in UvsX_{30–358} (Fig. 3a). A C316S mutation in the context of the full-length UvsX eliminated the dimeric species under oxidizing conditions (Fig. 3b). Note that the full-length dimer is present in the absence of oxidizing agent and is eliminated in the C316S mutant (Fig. 3b).

With some exceptions,^{36,37} RecA-like proteins crystallize in space group *P*6₁, reflecting their natural tendency to form filaments with approximately 6-fold screw axes. Based on other recombinase structures, we assumed that UvsX_{30–358} is missing the protein-protein interaction region at the N-terminus and therefore is unable to form active filaments. This proved to be correct. In the UvsX_{30–358} structure, the *P*6₁ crystal packing does not recapitulate the natural filament, and the *P*6₁ crystal filament is constructed from two UvsX monomers. Chain A actually creates the filament, and chain B decorates the filament with no interactions with its own symmetry mates (Fig. 2b). Interfilament crystal contacts are mediated by a third UvsX_{30–358}–UvsX_{30–358} interaction surface (1019.5 Å²) between β 10, β 11, and α 10 in chain A, and between α 4, α 5, α 7, and the loop connecting β 7 and β 8 in chain B.

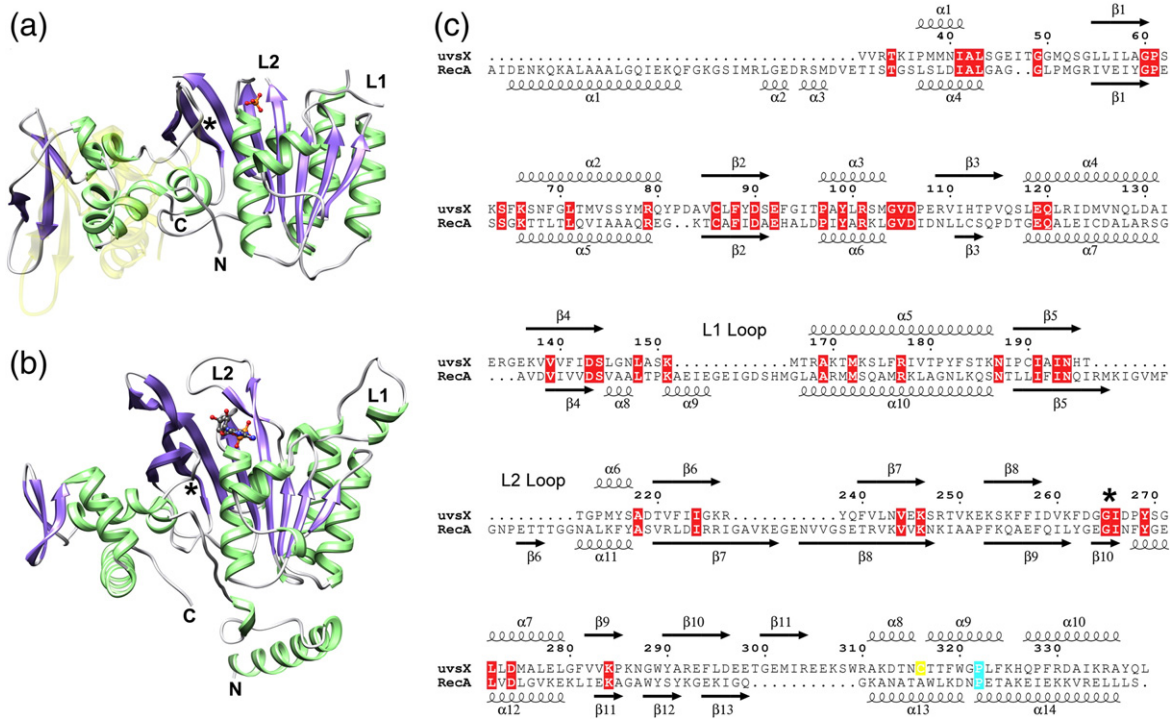


Fig. 1. Comparison of the UvsX₃₀₋₃₅₈ monomer with RecA. (a) The structure of the UvsX₃₀₋₃₅₈ monomer. α -Helices are shown in green, β -strands are shown in purple, and loops are shown in gray. The N-terminal ATP-binding $\alpha\beta$ core domain is oriented towards the right, and the helical C-terminal domain is on the left. ATP is not present in the structure, but the phosphate group (orange/red ball-and-stick) occupies the pocket that accommodates the ATP β -phosphate. Loops L1 and L2 are not visible in the structure, but their locations are labeled together with the N-terminus and the C-terminus. (b) The RecA monomer as determined by Chen *et al.* (Protein Data Bank code 3CMX), shown in the same orientation as UvsX in (a) based on an alignment of the core domain secondary structures.⁹ The RecA structure includes loops L1 and L2 (labeled) and a bound ADP (ball-and-stick). Note that the N-terminal oligomerization α -helix that was removed in UvsX to facilitate crystallization is present in RecA. (c) Structure-based sequence alignment of UvsX and RecA derived from (a) and (b). Sequence numbering refers to UvsX. Cys316 in UvsX is highlighted in yellow; RecA Pro313 and UvsX Pro322 are marked in cyan; and other identical residues are marked with red boxes. The figure was prepared with ESPript.³⁴ In (a), the semitransparent yellow structure shows the predicted location of the C-terminal domain based on its location in RecA. The ~15° rotation between the observed position and the predicted position occurs around a conserved Gly-Ile motif indicated by an asterisk in (a), (b), and (c).

The UvsX ATPase domain

Superposition of the UvsX and RecA⁹ structures reveals that the ATP binding site of UvsX is conserved both in terms of location (Fig. 1a and b) and in terms of residue composition (Fig. 1c). The Walker A or 'P loop' of RecA encompasses residues 65–73 and is equivalent to residues 59–67 of UvsX. The Walker B motif of RecA (residues 139–144) is also present in UvsX (residues 138–143) and contains the highly conserved aspartic acid (Asp144 in RecA; Asp143 in UvsX) that coordinates Mg²⁺ in the ATP complex. In RecA, the ATP adenine ring π -stacks with Tyr103, and Tyr99 of UvsX is suitably located to perform the equivalent function. Finally, the catalytic glutamic acid in RecA (Glu96) corresponds to Glu92 in UvsX. In RecA, the loop encompassing residues 261–269

encloses the adenine and ribose moieties of ATP, but the equivalent loop in UvsX (residues 259–267) is not suitably positioned in our structure to perform this role. This suggests that ATP is required to fix its position, although we note that this loop is poorly defined in our structure and located at the dimer interface where its conformation is probably distorted. Most notably, Tyr264 in RecA interacts closely with the adenine ring, but its probable functional counterpart in UvsX (Phe262) is not visible. In our dimer structure of UvsX, the ATP binding site is occluded at the dimer interface, which likely explains why we have not been able to introduce nucleotide into our crystals. However, each Walker A motif contains strong electron density consistent with a bound phosphate group that occupies the β -phosphate binding site of ATP (Fig. 1a and b).

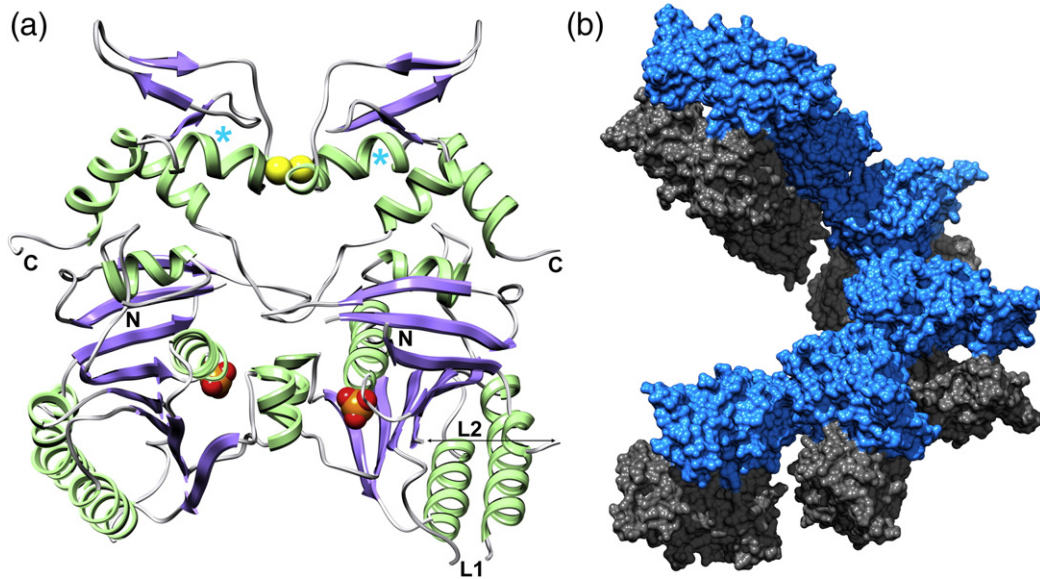


Fig. 2. The dimeric arrangement of UvsX₃₀₋₃₅₈ in the crystal asymmetric unit. (a) UvsX₃₀₋₃₅₈ is colored as in Fig. 1a. The ATP binding sites are indicated by the phosphate groups (orange/red CPK) and are occluded at the dimer interface. The paired Cys316 residues at the dimer interface appear to form a partially occupied disulfide bridge (yellow CPK) in the crystal and in solution (see Fig. 3). The positions of the N-terminus, the C-terminus, and loops L1 and L2 are indicated. The positions of Pro322 highlighted in Fig. 1c are marked with cyan asterisks. (b) Six dimers create one turn of a helical array in the *P*₆₁ unit cell. Interactions between successive monomer A molecules (blue) mediate the helical filament with no contributions from monomer B (gray).

EM reconstruction of UvsX filaments

Reconstructions of UvsX–DNA filaments from EM were analyzed several years ago,³⁸ and these images were reanalyzed using the UvsX crystal structure. UvsX filaments formed on dsDNA in the presence of ATP and aluminum fluoride possess structural heterogeneity. A data set of 3833 images analyzed using the Iterative Helical Real-Space Reconstruction

(IHRSR) procedure³⁹ did not converge into one unique solution. After sorting of the images by twist based on the pitch of the one-start helix, two classes emerged with twists of 6.2 U/turn and 7.0 U/turn. After 60 iterations, the most populated class (2154 images) converged into a filament with a rotation per subunit of 58.5° (6.15 U/turn) and an axial rise per subunit of 16.1 Å (pitch, 99 Å). UvsX filaments formed on dsDNA in the presence of ADP are

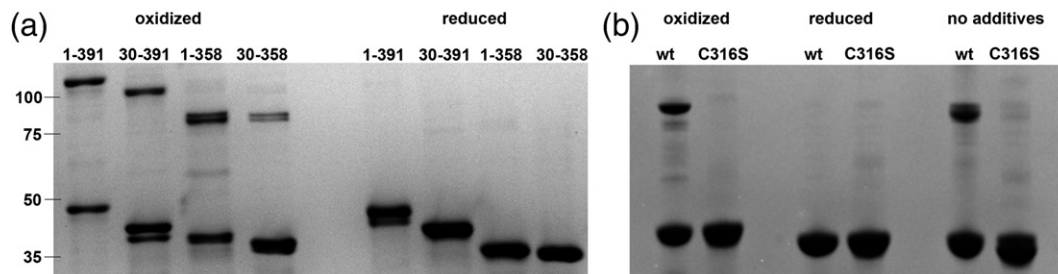


Fig. 3. SDS-PAGE analysis of oxidized and reduced UvsX. (a) Wild-type full-length and truncated UvsX proteins show partial dimerization when oxidized and a single band when reduced. The N-terminal deletion mutant UvsX₃₀₋₃₉₁ shows degradation when oxidized, but the reduced sample runs as a single species. The C-terminal deletion mutant UvsX₁₋₃₅₈ and the core domain UvsX₃₀₋₃₅₈ migrate similarly on the gel. The band positions of protein standards are marked with their molecular masses (kDa) on the left. Note that the dimeric fractions of both samples lacking the disordered acidic C-terminal region run at a molecular mass more consistent with the calculated molecular mass. The calculated molecular masses for each dimer are: 93 kDa for UvsX₁₋₃₉₁, 86 kDa for UvsX₃₀₋₃₉₁, 84 kDa for UvsX₁₋₃₅₈, and 80 kDa for UvsX₃₀₋₃₅₈. (b) The C316S point mutant of the full-length UvsX fails to dimerize under oxidizing conditions. Wild-type (wt) UvsX exhibits dimerization in the loading buffer without addition of oxidizing agents (right-hand side). Reduced UvsX protein was supplemented with 5 mM tris (2-carboxyethyl) phosphine, and oxidized protein was supplemented with 1% H₂O₂.

structurally more homogeneous and compressed than those formed in the presence of ATP and aluminum fluoride. Sorting by pitch revealed very small deviations from the mean value of 70 Å, and a data set of 3898 images was used in the IHRSR procedure that yielded a filament with a rotation per subunit of 55.7° (6.46 U/turn) and an axial rise per subunit of 10.8 Å (pitch, 69.8 Å). The three-dimensional reconstructions of the extended and compressed filaments are shown in Fig. 4a and b, respectively.

The crystal structure of UvsX was docked into the ATP/aluminum fluoride filament without any perturbations, yielding the atomic model of the UvsX filament in the extended state (Fig. 4a, cyan ribbons). The UvsX structure is lacking the first 30 residues, and there was a corresponding empty region of the envelope on the top of each protomer. We aligned a subunit from the crystal structure of the RecA active filament⁹ with the UvsX protomer, and the first 28 residues of RecA (shown as green ribbons in Fig. 4a) nicely filled the empty density in our reconstruction. The crystal structure of the RecA filament revealed that the ATP binding site sits at the monomer interface, with residues 248'–254' from the adjacent monomer providing a platform that encloses the exposed surface of the adenine and ribose rings. Also, Lys248' and Lys250' reach across the interface to form salt-bridge interactions with the ATP phosphate groups and the active site Glu96 (Fig. 5a). In the context of the UvsX EM reconstruction, these interactions are all present and mediated by residues 246'–252', Lys246', Arg248', and Glu92,

respectively (Fig. 5b). Thus, the EM reconstruction of the UvsX active filament is entirely consistent with the active RecA filament crystal structure.

The same docking procedure was used to build an atomic model of the UvsX filament in the compressed state (Fig. 4b, blue ribbons). The protomers are located at a higher radius than those in the extended state, but the overall relative orientation of adjacent protomers is very similar to that in the extended filament, with the missing N-terminus being able to mediate their interaction. The reconstruction shows density linking the ATPase core and the C-terminal lobe of adjacent protomers in successive turns of the helix (Fig. 4b, red arrows), which may stabilize the compressed filament, and the atomic model reveals that this is mediated by residues 130–132 and 285–288, respectively. One difference between compressed filaments and elongated filaments is the environment of the ATP binding site at the protomer interface. The 248'–254' platform that encloses the adenine and ribose moieties has moved by 4 Å and is replaced by the C-terminus of helix α6. This suggests that nucleotide is less easily accommodated at the protomer interface in the compressed filament.

The role of UvsW in the UvsX-promoted strand-exchange reaction

We next analyzed the UvsX-promoted strand-exchange reaction using 5.4-kb duplex linear DNA and homologous single-stranded circles (Fig. 6a).

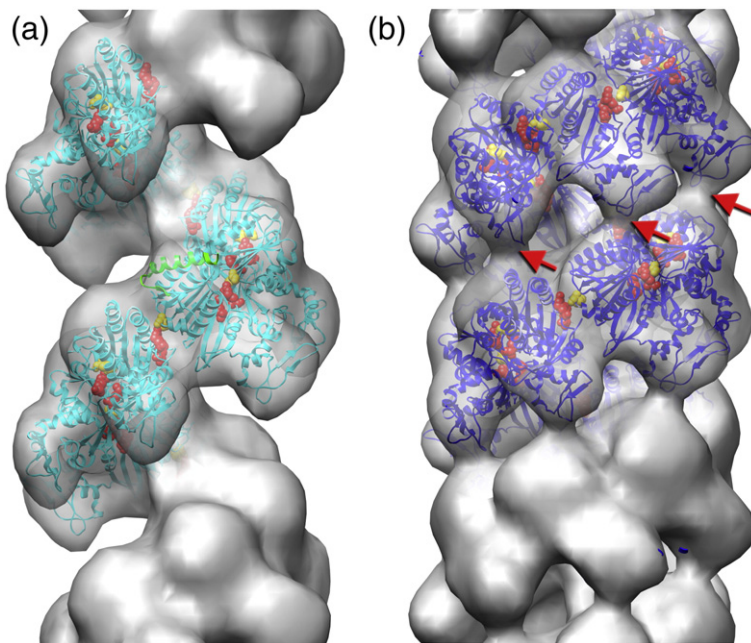


Fig. 4. EM of UvsX recombination filaments. (a) Reconstruction of the extended 'active' filament (gray) formed in the presence of dsDNA and ATP into which the UvsX crystal structure has been fitted (cyan). The C-terminal helical domain points down towards the large groove. The filament has a rotation per subunit of 58.5° and an axial rise per subunit of 16.1 Å. The 28 N-terminal residues of RecA were used to model the missing N-terminal UvsX residues (green ribbons). The positions of three residues in UvsX at the monomer-monomer interface that correspond to those in RecA involved in the ATP hydrolysis are shown as red (Lys246 and Arg248) and yellow (Glu92) spheres. (b) The compressed 'inactive' filament formed in the presence of dsDNA and ADP, where the fitted UvsX structure is

shown in dark blue. The filament has a rotation per subunit of 55.7° and an axial rise per subunit of 10.8 Å. A bridge of density across the groove, corresponding to an interaction between residues 130 and 132 of one monomer and between residues 285–288 of the other monomer, is indicated by red arrows.

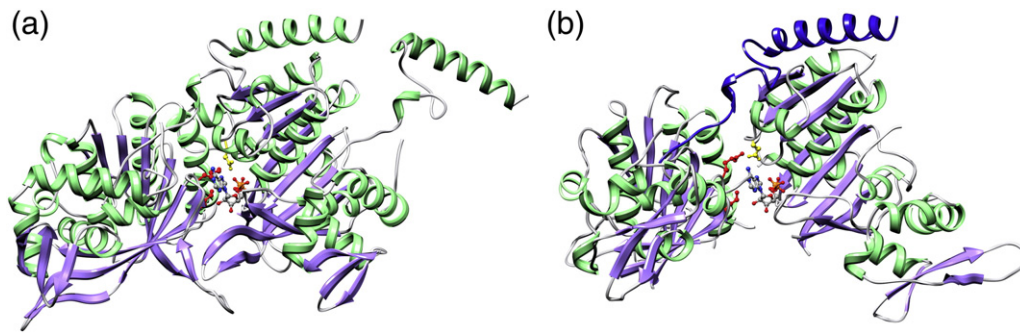


Fig. 5. Monomer–monomer interactions in the RecA and UvsX active filaments. (a) RecA–RecA interaction derived from the structure of Chen *et al.*⁹ ADP is bound at the interface, and the residues involved in ATP hydrolysis—Lys248 (red), Lys250 (red), and Glu96 (yellow)—are indicated. (b) The UvsX–UvsX interaction derived from the EM reconstruction. The ADP at the interface and the missing N-terminal α -helix (dark blue) are modeled from the RecA superposition shown in Fig. 1b. By comparison with the RecA structure, residues Lys246 (red), Arg248 (red), and Glu92 (yellow) mediate ATP hydrolysis at the interface.

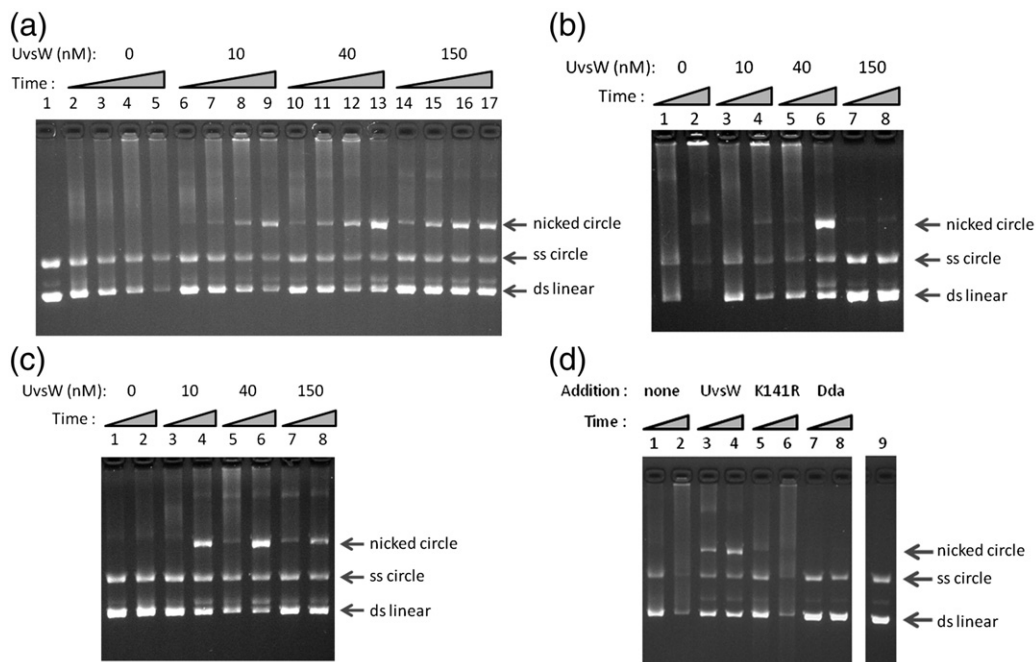


Fig. 6. UvsW allows completion of UvsX-promoted strand exchange. The migrations of nicked circular markers, single-stranded circular markers, and double-stranded linear markers are indicated by arrows at the right (top to bottom, respectively). (a) Strand-exchange reactions contained UvsX (1 μ M), UvsY (0.5 μ M), gp32 (2.5 μ M), and the indicated concentration of UvsW, along with the DNA substrates (linear duplex DNA and homologous single-stranded circles). Samples were removed at the following times: 2.5 min (lanes 2, 6, 10, and 14), 5 min (lanes 3, 7, 11, and 15), 10 min (lanes 4, 8, 12, and 16), and 22.5 min (lanes 5, 9, 13, and 17). The reaction in lane 1 contained UvsX, UvsY, and gp32, but not ATP. (b) UvsW allows completion of UvsX-promoted strand exchange in the absence of UvsY. Strand-exchange reactions contained UvsX and gp32 (each at 2.5 μ M), the indicated concentration of UvsW, and no UvsY protein. Samples were removed at 5 min (lanes 1, 3, 5, and 7) and 22.5 min (lanes 2, 4, 6, and 8). (c) UvsW promotes strand exchange under conditions where UvsY is inhibitory. Strand-exchange reactions contained UvsX, UvsY, gp32 (each at 2.5 μ M), and the indicated concentration of UvsW. Samples were removed at 5 min (lanes 1, 3, 5, and 7) and 22.5 min (lanes 2, 4, 6, and 8). (d) Dda helicase and UvsW-K141R do not facilitate completion of UvsX-promoted strand exchange. Strand-exchange reactions contained UvsX (2.5 μ M), UvsY (0.5 μ M), gp32 (2.5 μ M), and, where indicated, UvsW (50 nM), UvsW-K141R (50 nM), or Dda (75 nM). Samples were removed at 5 min (lanes 1, 3, 5, and 7) and 25 min (lanes 2, 4, 6, and 8). The reaction in lane 9 was a control that contained UvsX, UvsY, and gp32, but not ATP.

Similar to results from past studies,^{20,21,40,41} reactions containing UvsX, UvsY, and gp32 generated a smear of slowly migrating forms and DNA networks that do not enter the gel. These have been previously characterized as partial strand-exchange products containing multiple exchanges.⁴² Strikingly, the addition of UvsW protein at nanomolar concentrations allowed the robust generation of the complete strand-exchange product, nicked circular DNA (Fig. 6a, lanes 6–17). This result argues that UvsX is limited in its ability to promote branch migration during strand exchange, and that UvsW fulfills this role. UvsW promoted the formation of a nicked circular product under a variety of concentrations of UvsX, UvsY, and gp32 (Fig. 6; data not shown). UvsW could promote the formation of a nicked circular product by UvsX and gp32 in the absence of UvsY (Fig. 6b), showing that UvsY is not required for the stimulatory effect of UvsW. High concentrations of UvsY can also inhibit the reaction,⁴¹ under these conditions, the strand-exchange reaction was strikingly rescued by the presence of UvsW. Once again, the reaction proceeded to complete the nicked circular product (Fig. 6c).

We conclude that UvsW can stimulate the strand-invasion reaction and plays a major role in heteroduplex extension (three-strand branch migration) after the initial strand invasion. As expected, the inactive mutant UvsW-K141R did not promote the formation of a nicked circular product (Fig. 6d). Similar to a previous report,⁴³ the T4 Dda helicase inhibited the strand-invasion reaction and did not promote the formation of a nicked circular product (Fig. 6d). Finally, we found that high concentrations (e.g., 150 nM) of UvsW can inhibit the strand-exchange reaction (Fig. 6a–c). Thus, as with the other three components of the T4 strand-exchange system, the efficiency of the reaction depends exquisitely on the balance of protein concentrations.^{20,40,41}

Discussion

In this study, we report the crystal structure of the T4 recombinase UvsX and show that it closely resembles the structure of RecA. Moreover, using EM reconstructions, we demonstrate that the monomer–monomer interactions that mediate the ‘active’ recombination filament in T4 are very similar to those that mediate the RecA active filament. In terms of its primary structure, this close similarity to RecA was not particularly apparent,³⁵ although the structural homology was predicted.⁴⁴ The structural similarities justify the use of the T4 system to study the molecular basis of homologous recombination. Our structures of the T4 filament in both the extended ‘active’ conformation and the compressed ‘inactive’ conformation, together with the *in vitro* assay described in this report incorporating the

required T4 accessory proteins, will facilitate future studies to probe this key event.

The binding of ATP and ssDNA appears to stabilize an extended conformation of the filament that facilitates the strand-exchange process, and subsequent ATP hydrolysis generates an ADP-bound compressed filament that more readily disassembles. Insights into the transition between the two conformations and the roles of ATP hydrolysis and DNA tension in controlling this transition have recently been provided by single-molecule studies on Rad51^{45–47} and RecA.⁴⁸ Crystallographic analyses of RecA filaments have also revealed how ATP binding at the protomer–protomer interface stabilizes the extended filament in the presence of ssDNA.⁹ Although the molecular details of how these filament dynamics mediate the actual recombination reaction remain unclear, our structural studies on UvsX support a common fundamental mechanism for the DNA recombinase family. Compared to higher organisms, T4 recombination is relatively unencumbered by control mechanisms and accessory proteins, and is thus well suited for mechanistic analyses.

Does the crystallographic dimer have biological relevance? Our crystal-yielding UvsX_{30–358} construct lacks the N-terminal multimerization segment, and the dimer may therefore be an artifact. Comparison with the RecA structure supports this. In RecA, Pro313 is at the N-terminus of an α -helix (α 14) that forms part of a three-helix bundle within the C-terminal domain (Fig. 1c). In UvsX, this proline appears to be conserved as Pro322 but is located within helix α 9 (Figs. 1c and 2a), and the three-helix bundle is not present. The Cys316-mediated disulfide bond may therefore distort the three-helix bundle and place Pro322 within α 9. The formation of the crystal dimer also requires that the C-terminal domain be rotated by some 15° relative to that of RecA to avoid steric clash (Fig. 1a), but this rotation may reflect a functionally required flexibility between the two domains. The rotation occurs around a conserved Gly-Ile motif located at residues 266–267 (residues 267–268 in RecA) in the loop connecting β 8 in the core domain with α 7 in the C-terminal domain (Fig. 1). There is evidence that the C-terminal domain of RecA engages dsDNA during recombination,⁴⁹ and a flexible connecting loop would facilitate the docking of dsDNA within the filament in the manner suggested by Shin *et al.*³⁶

However, the possibility that the dimer may resemble a functional state of UvsX remains. We consistently detect a UvsX dimer in solution (Fig. 3), and the nonconserved Cys316 at the dimer interface may serendipitously stabilize it and allow its detection. We also note that the missing N-terminal multimerization α -helix would be located on the outer surface of the crystal dimer and would not prevent its formation (Fig. 2a). The dimer may

represent a storage form of UvsX in solution, as proposed for the heptameric and octameric double rings of the *Pyrococcus furiosus* RadA³⁶ and the human Dmc1,⁵⁰ that requires interaction with gp32 and ATP to form filaments on DNA. RecA dimers have been invoked in filament assembly,^{51,52} although other studies suggest that assembly occurs by the addition of monomers.⁶

We have demonstrated that UvsW helicase promotes the strand-exchange reaction catalyzed by UvsX in the presence or in the absence of UvsY. UvsW can both stimulate the overall level of strand invasion and promote the generation of the final product, nicked circular DNA. Past biochemical studies of UvsX revealed mostly complex DNA networks resulting from multiple incomplete strand-exchange reactions.¹ Thus, UvsW fills an important role in the T4 recombination reaction, allowing efficient branch migration during the early three-strand phase of the reaction (Fig. 6) and after the generation of an HJ.²⁶ Because UvsW unwinding activity is specific for branched DNA,^{25,26,30} we presume that it functions directly at the branch point during these reactions.

We recently demonstrated a structural similarity between UvsW and eukaryotic Rad54 protein,³³ suggesting that the core recombinatorial triad of Rad51/Rad52/Rad54 in eukaryotic cells is functionally equivalent to the UvsX/UvsY/UvsW triad in T4. Our current studies extend this apparent functional parallel between the two triads. Thus, Rad54, similar to UvsW, has been shown to both stimulate Rad51-dependent strand exchange and increase the levels of strand invasion.^{53–56} Also, in addition to promoting strand exchange between a double-stranded substrate and a single-stranded substrate, Rad54 and UvsW have both been shown to catalyze HJ branch migration.^{26,56} With the crystal structures of UvsW, UvsX, and gp32⁵⁷ now available and with a robust *in vitro* assay to monitor T4 recombination, we are now positioned to investigate how these three proteins interact at the molecular level to catalyze homologous recombination with the assistance of the RMP UvsY.

Materials and Methods

Cloning, expression, and purification of UvsX

The full-length *UvsX* gene was PCR amplified from phage T4 genomic DNA and subcloned into a pET28b expression vector (Novagen) with an N-terminal 6× His tag and a thrombin cleavage site. BL21 DE3 cells transformed with this vector were grown in LB media to an OD₆₀₀ of 0.6 and induced with 1 mM IPTG overnight at 16 °C. The cells were harvested by 20 min of centrifugation at 4000g, resuspended in lysis buffer [0.5 M NaCl, 50 mM NaPO₄ (pH 7.8), 40 mM imidazole, 10 mM

MgCl₂, and 10 mM β-mercaptoethanol], and lysed in a microfluidizer (Microfluidics). The lysate DNA was then digested for 30 min with DNase I (0.1 U/ml), followed by 30 min of centrifugation at 30,000g. The supernatant was loaded on a 5-ml Ni²⁺ chelation Sepharose column, and bound impurities were removed with 50 ml of equilibration buffer [0.5 M NaCl, 20 mM Tris-HCl (pH 8.0), 40 mM imidazole, and 5 mM β-mercaptoethanol]. This was followed by a linear gradient from 40 mM to 500 mM imidazole (20 column volumes) in the same buffer, during which essentially pure protein was eluted. The affinity tag was removed with thrombin (0.1 U/ml) digestion, and, following dialysis against equilibration buffer, the protein was passed over a 1-ml Ni²⁺ chelation Sepharose column to remove residual His-tagged UvsX. The protein was dialyzed against 175 mM NaCl and 20 mM Tris-HCl (pH 8.0), and further purified on a 25-ml Q Sepharose column using a linear elution gradient from 0.1 M to 1 M NaCl in 20 mM Tris-HCl (pH 8.0) and 5 mM β-mercaptoethanol (10 column volumes). The pooled fractions were estimated to be >98% pure by SDS-PAGE with Coomassie blue staining. For crystallization trials, the sample was dialyzed into 200 mM NaCl, 20 mM Tris-HCl (pH 8.5), and 2 mM DTT, concentrated to 15 mg/ml, flash frozen in liquid nitrogen, and stored at –80 °C.

Deletion mutants UvsX_{1–358}, UvsX_{30–391}, and UvsX_{30–358} were generated by PCR methods directly from the full-length expression construct. Using appropriate primers flanking the region to be deleted, we copied the entire expression plasmid minus the deletion and then resealed it via an engineered restriction site. The same technique was used to create the C316S point mutant within the full-length UvsX. UvsX_{30–358} labeled with SeMet was expressed as described elsewhere.⁵⁸ All the deletion mutants and the SeMet-labeled protein were purified using the protocol described above.

SDS-PAGE analysis of oxidized and reduced UvsX

UvsX proteins purified as described above were dialyzed exhaustively at 1–2 mg/ml concentration in a modified storage buffer [200 mM NaCl, 20 mM Tris-HCl (pH 8.5), and 0.5 mM ethylenediaminetetraacetic acid (EDTA)] without reducing agents. Proteins were oxidized by adjusting to a final concentration of 1% H₂O₂ and reduced to a final concentration of 5 mM Tris-(carboxyethyl)phosphine hydrochloride prior to 5 min of denaturation at 95 °C in 2% SDS, 20% glycerol, and 50 mM Tris-HCl (pH 6.8). Samples were run on 4–20% acrylamide gels and stained with Coomassie blue.

Crystallization, data collection, and structure solution of UvsX

Purified full-length UvsX and the truncated versions UvsX_{1–358}, UvsX_{30–391}, and UvsX_{30–358} were all subjected to crystallization screens. Native UvsX_{30–358} crystals grew to 0.2 mm × 0.2 mm × 0.6 mm within 3 weeks at 18 °C in 1.8 M ammonium sulfate, 0.2 M ammonium phosphate, 0.1 M Hepes (pH 8.0), and 5 mM DTT. None of the other protein variants yielded crystals, either in apo form or in the presence of ADP-Mg²⁺. Virtually identical SeMet-labeled

UvsX_{30–358} crystals grew within 4 days in 0.8 M succinate (pH 7.0), 0.1 M Hepes–Na (pH 8.0), and 5 mM DTT. Crystals were cryoprotected in their mother liquor supplemented with serially increasing concentrations of 10%, 25%, and 35% ethylene glycol prior to flash freezing in liquid nitrogen. Diffraction data were collected at Southeast Regional Collaborative Access Team beamline ID-22 (Advanced Photon Source, Argonne, IL). Native crystals diffracted to 2.4 Å resolution, and SeMet anomalous scattering data sets were collected to 2.8 Å resolution. The initial structure solution was obtained from the SeMet peak signal using the SAD method with the PHENIX software.⁵⁹ Model building was performed using Coot,⁶⁰ and the structure was refined at 2.4 Å against the native structure factors with a combination of CNS⁶¹ and Refmac⁶² using NCS restraints and TLS refinement.

Image analysis of UvsX filaments

EM images of UvsX–DNA complexes obtained by Yang *et al.* were used for the analysis.³⁸ Negatives were scanned with a Nikon Coolscan 8000 as 16-bit images using a raster of 4.2 Å/pixel. EMAN package was used to extract filament images from micrographs,⁶³ and overlapping segments (60 pixels long) of the filaments were collected from the images and used in the IHRSR procedure.³⁹ UCSF Chimera software⁶⁴ was used to fit crystal structures into the experimental maps. Atomic coordinates from crystal structures were converted into density maps, and these were filtered to the resolution of the experimental map and docked manually.

Strand-exchange reactions

Full-length UvsX protein was purified in one step with Ni²⁺ Sepharose affinity chromatography as described above, omitting thrombin cleavage and Q-Sepharose chromatography. UvsY was also expressed as an N-terminal 6×His-tagged fusion protein from a pET28b construct and purified on a Ni²⁺-chelating Sepharose column using the same buffers as described for UvsX. UvsX and UvsY were dialyzed into a storage buffer containing 500 mM NaCl, 20 mM Tris–HCl (pH 7.8), 1 mM DTT, 0.5 mM EDTA, and 10% (wt/vol) glycerol, and stored at –20 °C. UvsW was purified as previously described,²⁶ and gp32 was obtained from New England Biolaboratories. Strand-exchange reactions contained φX174 single-stranded circular DNA (15 μM in nucleotide), linearized φX174 double-stranded circular DNA (10 μM in nucleotide), the indicated T4 proteins, and an ATP regeneration system (2 mM ATP, 15 mM creatine phosphate, and creatine phosphokinase at 25 μg/ml) in a buffer consisting of 30 mM Tris–HCl (pH 7.8), 90 mM sodium acetate, 10 mM magnesium acetate, 1 mM DTT, and 0.1 mg/ml bovine serum albumin. Reactions were incubated at 37 °C for 2 min without ATP, and then initiated by the addition of ATP. At the indicated times, an aliquot was removed and treated with one-tenth volume of a 10× stop solution (100 mM EDTA, 5% SDS, 20% Ficoll, and 5 mg/ml proteinase K), followed by 10 min of incubation at 37 °C. The reaction products were separated by agarose gel electrophoresis and stained with ethidium bromide.

Accession codes

Structure factors and refined coordinates have been deposited in the Protein Data Bank under accession code 3IO5.

Acknowledgements

This work was supported by National Institutes of Health grants GM066934 (to S.W.W. and K.N.K.) and GM035269 (to E.H.E.), Cancer Center core grant CA21765, and the American Lebanese Syrian Associated Charities. Data were collected at Southeast Regional Collaborative Access Team beamline 22-ID at the Advanced Photon Source, Argonne National Laboratory. Supporting institutions may be found at www.ser-cat.org/members.html. Use of the Advanced Photon Source was supported by the US Department of Energy, Office of Science, Office of Basic Energy Sciences, under contract no. W-31-109-Eng-38. We thank Dr. Xiaoping He for providing the Dda protein.

References

1. Bianco, P. R., Tracy, R. B. & Kowalczykowski, S. C. (1998). DNA strand exchange proteins: a biochemical and physical comparison. *Front. Biosci.* **3**, D570–D603.
2. West, S. C. (2003). Molecular views of recombination proteins and their control. *Nat. Rev. Mol. Cell Biol.* **4**, 435–445.
3. Li, X. & Heyer, W. D. (2008). Homologous recombination in DNA repair and DNA damage tolerance. *Cell Res.* **18**, 99–113.
4. Cox, M. M., Goodman, M. F., Kreuzer, K. N., Sherratt, D. J., Sandler, S. J. & Marians, K. J. (2000). The importance of repairing stalled replication forks. *Nature*, **404**, 37–41.
5. San Filippo, J., Sung, P. & Klein, H. (2008). Mechanism of eukaryotic homologous recombination. *Annu. Rev. Biochem.* **77**, 229–257.
6. Joo, C., McKinney, S. A., Nakamura, M., Rasnik, I., Myong, S. & Ha, T. (2006). Real-time observation of RecA filament dynamics with single monomer resolution. *Cell*, **126**, 515–527.
7. Galletto, R., Amitani, I., Baskin, R. J. & Kowalczykowski, S. C. (2006). Direct observation of individual RecA filaments assembling on single DNA molecules. *Nature*, **443**, 875–878.
8. Prasad, T. K., Yeykal, C. C. & Greene, E. C. (2006). Visualizing the assembly of human Rad51 filaments on double-stranded DNA. *J. Mol. Biol.* **363**, 713–728.
9. Chen, Z., Yang, H. & Pavletich, N. P. (2008). Mechanism of homologous recombination from the RecA–ssDNA/dsDNA structures. *Nature*, **453**, 489–494.
10. Kreuzer, K. N. & Morrical, S. W. (1994). Initiation of DNA replication. In *Molecular Biology of Bacteriophage*

- T4 (Karam, J. D., ed.), pp. 28–42, ASM Press, Washington, DC.
11. Bleuit, J. S., Xu, H., Ma, Y., Wang, T., Liu, J. & Morrical, S. W. (2001). Mediator proteins orchestrate enzyme–ssDNA assembly during T4 recombination-dependent DNA replication and repair. *Proc. Natl Acad. Sci. USA*, **98**, 8298–8305.
 12. Mosig, G. (1994). Homologous recombination. In *Molecular Biology of Bacteriophage T4* (Karam, J. D., ed.), pp. 54–82, ASM Press, Washington, DC.
 13. Yu, X. & Egelman, E. H. (1993). DNA conformation induced by the bacteriophage T4 UvsX protein appears identical to the conformation induced by the *Escherichia coli* RecA protein. *J. Mol. Biol.* **232**, 1–4.
 14. Ando, R. A. & Morrical, S. W. (1998). Single-stranded DNA binding properties of the UvsX recombinase of bacteriophage T4: binding parameters and effects of nucleotides. *J. Mol. Biol.* **283**, 785–796.
 15. Yonesaki, T. & Minagawa, T. (1985). T4 phage gene uvsX product catalyzes homologous DNA pairing. *EMBO J.* **4**, 3321–3327.
 16. Formosa, T. & Alberts, B. M. (1986). DNA synthesis dependent on genetic recombination: characterization of a reaction catalyzed by purified bacteriophage T4 proteins. *Cell*, **47**, 793–806.
 17. Hinton, D. M. & Nossal, N. G. (1986). Cloning of the bacteriophage T4 uvsX gene and purification and characterization of the T4 uvsX recombination protein. *J. Biol. Chem.* **261**, 5663–5673.
 18. Harris, L. D. & Griffith, J. (1987). Visualization of the homologous pairing of DNA catalyzed by the bacteriophage T4 UvsX protein. *J. Biol. Chem.* **262**, 9285–9292.
 19. Beermink, H. T. & Morrical, S. W. (1999). RMPs: recombination/replication mediator proteins. *Trends Biochem. Sci.* **24**, 385–389.
 20. Yonesaki, T. & Minagawa, T. (1989). Synergistic action of three recombination gene products of bacteriophage T4, uvsX, uvsY, and gene 32 proteins. *J. Biol. Chem.* **264**, 7814–7820.
 21. Kodadek, T., Gan, D. C. & Stemke-Hale, K. (1989). The phage T4 uvsY recombination protein stabilizes presynaptic filaments. *J. Biol. Chem.* **264**, 16451–16457.
 22. Bleuit, J. S., Ma, Y., Munro, J. & Morrical, S. W. (2004). Mutations in a conserved motif inhibit single-stranded DNA binding and recombination mediator activities of bacteriophage T4 UvsY protein. *J. Biol. Chem.* **279**, 6077–6086.
 23. Liu, J., Bond, J. P. & Morrical, S. W. (2006). Mechanism of presynaptic filament stabilization by the bacteriophage T4 UvsY recombination mediator protein. *Biochemistry*, **45**, 5493–5502.
 24. Liu, J., Qian, N. & Morrical, S. W. (2006). Dynamics of bacteriophage T4 presynaptic filament assembly from extrinsic fluorescence measurements of Gp32–single-stranded DNA interactions. *J. Biol. Chem.* **281**, 26308–26319.
 25. Carles-Kinch, K., George, J. W. & Kreuzer, K. N. (1997). Bacteriophage T4 UvsW protein is a helicase involved in recombination, repair and the regulation of DNA replication origins. *EMBO J.* **16**, 4142–4151.
 26. Webb, M. R., Plank, J. L., Long, D. T., Hsieh, T. S. & Kreuzer, K. N. (2007). The phage T4 protein UvsW drives Holliday junction branch migration. *J. Biol. Chem.* **282**, 34401–34411.
 27. Hamlett, N. V. & Berger, H. (1975). Mutations altering genetic recombination and repair of DNA in bacteriophage T4. *Virology*, **63**, 539–567.
 28. Derr, L. K. & Drake, J. W. (1990). Isolation and genetic characterization of new uvsW alleles of bacteriophage T4. *Mol. Gen. Genet.* **222**, 257–264.
 29. Derr, L. K. & Kreuzer, K. N. (1990). Expression and function of the uvsW gene of bacteriophage T4. *J. Mol. Biol.* **214**, 643–656.
 30. Nelson, S. W. & Benkovic, S. J. (2007). The T4 phage UvsW protein contains both DNA unwinding and strand annealing activities. *J. Biol. Chem.* **282**, 407–416.
 31. Nelson, S. W., Perumal, S. K. & Benkovic, S. J. (2009). Processive and unidirectional translocation of monomeric UvsW helicase on single-stranded DNA. *Biochemistry*, **48**, 1036–1046.
 32. Sickmier, E. A., Kreuzer, K. N. & White, S. W. (2004). The crystal structure of the UvsW helicase from bacteriophage T4. *Structure*, **12**, 583–592.
 33. Kerr, I. D., Sivakolundu, S., Li, Z., Buchsbaum, J. C., Knox, L. A., Kriwacki, R. & White, S. W. (2007). Crystallographic and NMR analyses of UvsW and UvsW.1 from bacteriophage T4. *J. Biol. Chem.* **282**, 34392–34400.
 34. Gouet, P., Courcelle, E., Stuart, D. I. & Metz, F. (1999). ESPript: analysis of multiple sequence alignments in PostScript. *Bioinformatics*, **15**, 305–308.
 35. Fujisawa, H., Yonesaki, T. & Minagawa, T. (1985). Sequence of the T4 recombination gene, uvsX, and its comparison with that of the recA gene of *Escherichia coli*. *Nucleic Acids Res.* **13**, 7473–7481.
 36. Shin, D. S., Pellegrini, L., Daniels, D. S., Yelent, B., Craig, L., Bates, D. *et al.* (2003). Full-length archaeal Rad51 structure and mutants: mechanisms for RAD51 assembly and control by BRCA2. *EMBO J.* **22**, 4566–4576.
 37. Conway, A. B., Lynch, T. W., Zhang, Y., Fortin, G. S., Fung, C. W., Symington, L. S. & Rice, P. A. (2004). Crystal structure of a Rad51 filament. *Nat. Struct. Mol. Biol.* **11**, 791–796.
 38. Yang, S., VanLoock, M. S., Yu, X. & Egelman, E. H. (2001). Comparison of bacteriophage T4 UvsX and human Rad51 filaments suggests that RecA-like polymers may have evolved independently. *J. Mol. Biol.* **312**, 999–1009.
 39. Egelman, E. H. (2000). A robust algorithm for the reconstruction of helical filaments using single-particle methods. *Ultramicroscopy*, **85**, 225–234.
 40. Harris, L. D. & Griffith, J. D. (1989). UvsY protein of bacteriophage T4 is an accessory protein for *in vitro* catalysis of strand exchange. *J. Mol. Biol.* **206**, 19–27.
 41. Morrical, S. W. & Alberts, B. M. (1990). The UvsY protein of bacteriophage T4 modulates recombination-dependent DNA synthesis *in vitro*. *J. Biol. Chem.* **265**, 15096–15103.
 42. Kodadek, T., Wong, M. L. & Alberts, B. M. (1988). The mechanism of homologous DNA strand exchange catalyzed by the bacteriophage T4 uvsX and gene 32 proteins. *J. Biol. Chem.* **263**, 9427–9436.
 43. Kodadek, T. (1991). Inhibition of protein-mediated homologous pairing by a DNA helicase. *J. Biol. Chem.* **266**, 9712–9718.
 44. Story, R. M., Bishop, D. K., Kleckner, N. & Steitz, T. A. (1993). Structural relationship of bacterial RecA

- proteins to recombination proteins from bacteriophage T4 and yeast. *Science*, **259**, 1892–1896.
45. Hilario, J., Amitani, I., Baskin, R. J. & Kowalczykowski, S. C. (2009). Direct imaging of human Rad51 nucleoprotein dynamics on individual DNA molecules. *Proc. Natl Acad. Sci. USA*, **106**, 361–368.
 46. van Mameren, J., Modesti, M., Kanaar, R., Wyman, C., Peterman, E. J. & Wuite, G. J. (2009). Counting RAD51 proteins disassembling from nucleoprotein filaments under tension. *Nature*, **457**, 745–748.
 47. Robertson, R. B., Moses, D. N., Kwon, Y., Chan, P., Chi, P., Klein, H. *et al.* (2009). Structural transitions within human Rad51 nucleoprotein filaments. *Proc. Natl Acad. Sci. USA*, **106**, 12688–12693.
 48. Nishinaka, T., Doi, Y., Hashimoto, M., Hara, R., Shibata, T., Harada, Y. *et al.* (2007). Visualization of RecA filaments and DNA by fluorescence microscopy. *J. Biochem.* **141**, 147–156.
 49. Aihara, H., Ito, Y., Kurumizaka, H., Terada, T., Yokoyama, S. & Shibata, T. (1997). An interaction between a specified surface of the C-terminal domain of RecA protein and double-stranded DNA for homologous pairing. *J. Mol. Biol.* **274**, 213–221.
 50. Kinebuchi, T., Kagawa, W., Enomoto, R., Tanaka, K., Miyagawa, K., Shibata, T. *et al.* (2004). Structural basis for octameric ring formation and DNA interaction of the human homologous-pairing protein Dmc1. *Mol. Cell*, **14**, 363–374.
 51. Lauder, S. D. & Kowalczykowski, S. C. (1991). Asymmetry in the recA protein–DNA filament. *J. Biol. Chem.* **266**, 5450–5458.
 52. Forget, A. L., Kudron, M. M., McGrew, D. A., Calmann, M. A., Schiffer, C. A. & Knight, K. L. (2006). RecA dimers serve as a functional unit for assembly of active nucleoprotein filaments. *Biochemistry*, **45**, 13537–13542.
 53. Petukhova, G., Stratton, S. & Sung, P. (1998). Catalysis of homologous DNA pairing by yeast Rad51 and Rad54 proteins. *Nature*, **393**, 91–94.
 54. Solinger, J. A. & Heyer, W. D. (2001). Rad54 protein stimulates the postsynaptic phase of Rad51 protein-mediated DNA strand exchange. *Proc. Natl Acad. Sci. USA*, **98**, 8447–8453.
 55. Solinger, J. A., Lutz, G., Sugiyama, T., Kowalczykowski, S. C. & Heyer, W. D. (2001). Rad54 protein stimulates heteroduplex DNA formation in the synaptic phase of DNA strand exchange via specific interactions with the presynaptic Rad51 nucleoprotein filament. *J. Mol. Biol.* **307**, 1207–1221.
 56. Bugreev, D. V., Mazina, O. M. & Mazin, A. V. (2006). Rad54 protein promotes branch migration of Holliday junctions. *Nature*, **442**, 590–593.
 57. Shamoo, Y., Friedman, A. M., Parsons, M. R., Konigsberg, W. H. & Steitz, T. A. (1995). Crystal structure of a replication fork single-stranded DNA binding protein (T4 gp32) complexed to DNA. *Nature*, **376**, 362–366.
 58. Doublet, S. (1997). Preparation of selenomethionyl proteins for phase determination. *Methods Enzymol.* **276**, 523–530.
 59. Adams, P. D., Grosse-Kunstleve, R. W., Hung, L. W., Ioerger, T. R., McCoy, A. J., Moriarty, N. W. *et al.* (2002). PHENIX: building new software for automated crystallographic structure determination. *Acta Crystallogr. Sect. D*, **58**, 1948–1954.
 60. Emsley, P. & Cowtan, K. (2004). Coot: model-building tools for molecular graphics. *Acta Crystallogr. Sect. D*, **60**, 2126–2132.
 61. Brunger, A. T., Adams, P. D., Clore, G. M., DeLano, W. L., Gros, P., Grosse-Kunstleve, R. W. *et al.* (1998). Crystallography & NMR system: a new software suite for macromolecular structure determination. *Acta Crystallogr. Sect. D*, **54**, 905–921.
 62. Murshudov, G. N., Vagin, A. A. & Dodson, E. J. (1997). Refinement of macromolecular structures by the maximum-likelihood method. *Acta Crystallogr. Sect. D*, **53**, 240–255.
 63. Ludtke, S. J., Baldwin, P. R. & Chiu, W. (1999). EMAN: semiautomated software for high-resolution single-particle reconstructions. *J. Struct. Biol.* **128**, 82–97.
 64. Pettersen, E. F., Goddard, T. D., Huang, C. C., Couch, G. S., Greenblatt, D. M., Meng, E. C. & Ferrin, T. E. (2004). UCSF Chimera—a visualization system for exploratory research and analysis. *J. Comput. Chem.* **25**, 1605–1612.